

Anion- and Solvent-Induced Single-Crystal-to-Single-Crystal Transformation within an Iron(II) Triazole System: a Promising Luminescent Probe for CrO_4^{2-} and Cyano-Containing Molecules

Ying Wang,^{*,†,‡,⊕} Ran Chen,[†] Wei Jia,[†] Qian Wang,[†] Chong-Yu Xue,[†] Jia-Hui Fan,[†] Wan-Ru Qi,[†] Yue-Juan Qin,[†] Yu-Hua Pan,[†] and Rong-Rong Yang[†]

[†]Key Laboratory of Inorganic–Organic Hybrid Functional Material Chemistry, Ministry of Education, and Tianjin Key Laboratory of Structure and Performance for Functional Molecules, Tianjin Normal University, Tianjin 300387, China

[‡]Key Laboratory of Advanced Energy Materials Chemistry (Ministry of Education), Nankai University, Tianjin 300071, China

Supporting Information

ABSTRACT: Anion- and solvent-induced single-crystal-to-single-crystal transformation within an iron(II) triazole system has been generated from $\{[\text{Fe}(\text{TPPT})_2\text{Cl}_2] \cdot \text{CHCl}_3\}_n$ (**1a**) to $[\text{Fe}(\text{TPPT})(\text{C}_2\text{O}_4)_{0.5}\text{Cl}(\text{H}_2\text{O})]_n$ (**1b**). Luminescence studies indicated that the resultant **1b** can be considered as a promising luminescent probe for CrO_4^{2-} and cyano molecules.

Metal–organic frameworks (MOFs) have served as a new type of material in anionic pollutant elimination, gas sensing, catalysis, chemical separation, biomedicine, molecular recognition, selective anion exchange, sensing, etc.¹ The ultimate topology of MOFs is mostly influenced by many factors, including captured guest molecules, the oxidation state of the metal ion, and changes of the coordination number owing to the formation and breakage of new chemical bonds. Therefore, MOF crystals are inclined to undergo single-crystal-to-single-crystal (SC–SC) structural transformations. Many factors influence the dynamic process of SC–SC transformation, which can afford accurate imagery about structural alterations during the transitions.² Hence, a structure–property relationship can be well illustrated by monitoring the transformation process. So far, a number of MOFs have been reported to experience solid-phase conversions in response to outside stimuli, for example, heat, light, redox reaction, chemical reactions, and guest exchange.³ These structural changes usually included lattice distortion, molecular conformational twisting or folding, variations in the metalphilicity, hydrogen-bonding or other supramolecular interactions, and guest component inclusion or exclusion. Meanwhile, this process is often accompanied by a distinct change in the functions.⁴

Following the rapid development of industry and agriculture, heavy-metal pollution has become a global environmental problem and severely threatens biological diversity and people's health.⁵ In particular, hexavalent chromium (Cr^{VI}) is a typical carcinogen existing in industrial sewage from alloying, electric plating, and metal buffing. Thus, eliminating Cr^{VI} from effluents is urgent. As is well-known, in the past few years, cyanide deaths have been on the rise. Because of the strong electronic recycling ability of CN^- , cyano moieties display high reactive activity.⁶ However, cyano-containing molecules are assumed to be the

intermediate product of the constitution of biorelated molecules, while these compounds have not been shown to replicate the retrovirus, which is not toxic to host cells. A hemohemin system can be obtained from the strong ligand CN^- , causing the heme to enter a low-spin state, which is usually considered to be very steady and does not occur in light decomposition.⁷ Hence, it is very important from the point of view of environmental and security considerations to discover the luminescent probes for cyano moieties and CrO_4^{2-} . Inspired by our previous work,⁸ we now try to construct a 1D double chain $\{[\text{Fe}(\text{SCN})_2(\text{TPPT})_2] \cdot 2\text{CH}_3\text{OH}\}_n$ (**1**) by using 1-{4-[4-(1*H*-1,2,4-triazol-1-yl)-phenoxy]phenyl}-1*H*-1,2,4-triazole (TPPT) as a building block for self-assembly with NH_4SCN and $\text{FeCl}_2 \cdot 4\text{H}_2\text{O}$ in a $\text{H}_2\text{O}/\text{CHCl}_3/\text{CH}_3\text{OH}$ mixed solution. Dynamic transformation results indicated that SCN^- in the 1D ferrous framework **1** could be completely exchanged by Cl^- through a SC–SC transformation process, as evidenced by the anion- and solvent-exchanged products of $\{[\text{Fe}(\text{TPPT})_2\text{Cl}_2] \cdot \text{CHCl}_3\}_n$ (**1a**). Further, if **1a** were employed as a precursor in an aqueous solution of $\text{K}_2\text{C}_2\text{O}_4$, a 2D layer of $[\text{Fe}(\text{TPPT})(\text{C}_2\text{O}_4)_{0.5}\text{Cl}(\text{H}_2\text{O})]_n$ (**1b**) could be generated after partially anion-exchanged and completely solvent-exchanged reactions. Magnetic investigations of **1b** indicate the presence of weak antiferromagnetic coupling between Fe^{II} ions. More interestingly, the luminescent properties reveal that **1b** can detect CrO_4^{2-} and cyano molecules with relatively high sensitivity and selectivity.

The ligand TPPT was synthesized by a method reported in the literature.^{8c} Single-crystal X-ray diffraction analysis demonstrates that **1** features a 1D double chain (Figure S2), which belongs to the triclinic system with a $P\bar{1}$ space group. As shown in Figure S3, the Fe^{II} ion has a slightly distorted octahedral coordination environment with four $\text{N}_{\text{triazole}}$ atoms (N3, N3A, N6A, and N6B) from four TPPT ligands in the equatorial plane and two N atoms (N7 and N7A) from two SCN^- anions in the axial direction. The bond lengths of $\text{Fe}^{\text{II}}-\text{N}$ are 2.145(2), 2.207(2), and 2.347(9) Å, all of which are in the normal range of the observed ferrous complexes.⁹ The corresponding dihedral angles between the benzene and triazole rings in **1** are 26.5 and 26.9°, much less than that of two terminal triazole groups (76.6°). The flexible dihedral angles between the triazole and benzene moieties indicate

Received: December 8, 2017

different spatially distorted effects for coordination with the Fe^{II} ions and dictate the direction of chain extension. Such delicate factors are significant for determining the resultant construction of the self-assemblies. The Fe^{II} nodes are connected to each other through TPPT to form an infinite 1D double chain that consists of a 32-membered macrocycle-containing building block (Figure S4). In each rectangular ring, the $\text{Fe}\cdots\text{Fe}$ contact is around 16 Å, whereas the opposite phenoxy $\text{O}\cdots\text{O}$ distance is approximately 11 Å. 1D macrocycle-containing double chains stack together in an $-AA-$ fashion and form distorted quadrangle-like channels. CH_3OH as guest molecules have been encapsulated in these channels. Analysis of the crystal packing of **1** reveals the existence of two intermolecular $\text{O}\cdots\text{H}\cdots\text{O}$ hydrogen bonds, including $\text{O2}\cdots\text{S1}^{\text{i}}$ (i: $-1 + x, -1 + y, -z$) and $\text{O2}\cdots\text{S1}^{\text{ii}}$ (ii: $-1 - x, -1 - y, -z$) between the uncoordinated methanol molecule and S atoms from SCN^- terminal ligands. The $\text{O}\cdots\text{S}$ separations are in the 3.3243(4)–3.5984(3) Å range and the $\text{H}\cdots\text{O}$ distances in the 2.5848(3)–3.0364(3) Å range. The bond angles are in the region of 127.8598(10)–150.716(8)°, being in the normal range of such weak interactions.¹⁰ Therefore, these mononuclear units are connected through hydrogen bonds to form a 3D supramolecular pattern, as depicted in Figure S5.

Encouraged by the previous progress in the study of SC–SC transformation,⁸ in this work, **1**, as a precursor, was immersed in a $\text{H}_2\text{O}/\text{CH}_3\text{OH}/\text{CHCl}_3$ mixed solution of NaCl to yield brown block crystals of **1a**, while maintaining the crystallinity throughout. There was no apparent change in the shape and color of the crystals, as displayed in Figure S6. Powder X-ray diffraction (PXRD) patterns indicated the phase purity before and after SC–SC transformation (Figure S7). Single-crystal X-ray diffraction analysis indicates that **1a** crystallizes in the orthorhombic $Pbcn$ space group. It is noted that the coordination modes for the TPPT ligands in **1a** are different from those in **1** (Figure S8), in which the two apically coordinated N_{SCN} atoms are completely replaced by two Cl^- anions. This substitution was probably triggered by the thermodynamics of coordination. The corresponding dihedral angles between the benzene and triazole moieties are 34 and 12.4°, while the dihedral angle between the two terminal triazole rings is 82.4°, indicating that the terminal triazole groups on each *cis*-TPPT ligand are basically perpendicular to each other and have much stronger spatial distortion than that of **1**.

Each Fe^{II} ion in **1a** connects four TPPT ligands and each TPPT links two Fe^{II} ions, leading to a 2D 3-fold-interpenetrated architecture (Figure 1). As shown in Figure S9, dissociative CHCl_3 guest molecules are located in the 1D quadrangle-like channels, in which the solvent-accessible void in **1a** is ca. 17.7%, as estimated by PLATON.^{11a} To understand the whole structure of **1a** more clearly, its topological structure is achieved by the

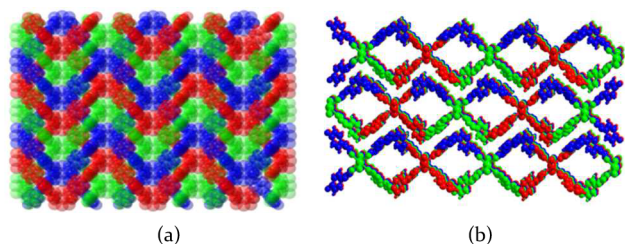


Figure 1. 3-fold-interpenetrated architecture of **1a** along the *c* axis (a) and along the *a* axis (b). Blue, red, and green indicate the 2D 3-fold-interpenetrated layers.

application of topology analysis via the freely available computer program TOPOS.^{11b} If each Fe^{II} ion is viewed as the 4-connected node, the 2D framework of **1a** can be described as a 3-fold-interpenetrated (4,4) net (Figure S10).

Interestingly, when **1a** was employed as a precursor in an aqueous solution of $\text{K}_2\text{C}_2\text{O}_4$ for 6 h, the exchanged product of **1b** was obtained. Complex **1b** is only accessible through anion- and solvent-induced SC–SC transformation from complex **1a** as a precursor, instead of from complex **1**. In the resultant complex **1b**, the incorporated oxalate plays the role of a pillar bridging two Fe^{II} sites, thus generating a 2D layer structure. The distance between the two connected Fe^{II} sites is 5.642 Å. Meanwhile, the closest distances between two adjacent Fe^{II} sites in **1** and **1a** are 11.939 and 7.583 Å, respectively. It can be concluded that changing from SCN^- of **1** to Cl^- of **1a** shortens the distance between the two Fe^{II} sites, which facilitates the incorporation of oxalate as the second-step SC–SC transformation. In the process of SC–SC transformation from **1a** to **1b**, we confirmed leaching of the TPPT ligand from the crystal to the solution by ^1H NMR, which was displaced by the embedded oxalate ligand. Thus, SC–SC transformation access to **1b** can be tentatively proposed by anion exchange from SCN^- to Cl^- and the incorporation of oxalate to displace one TPPT ligand on each Fe^{II} site. The anion exchange step is essential to the generation of **1b** because of shrinkage of the distance between the two chains.

Single-crystal X-ray diffraction analysis shows that **1b** crystallizes in the monoclinic system with the $P2(1)/c$ space group. As shown in Figure S11, the fundamental unit contains one crystallographically independent Fe^{II} ion. Fe1 is situated in the center of a distorted octahedron environment, with two $\text{N}_{\text{triazole}}$ atoms (N3 and N6A) located at the axial positions. Two O atoms (O2 and O3A) from $\text{C}_2\text{O}_4^{2-}$, one water molecule (O4), and one chloride ion (Cl1) are situated at the equatorial sites. The $\text{Fe}\text{--}\text{N}$ and $\text{Fe}\text{--}\text{O}$ distances are 2.187(0), 2.159(0), 2.116(1), and 2.191(1) Å, while the bond length of $\text{Fe}\text{--}\text{Cl}$ is 2.428(1) Å, all of which are in the normal range of those observed in ferrous complexes.⁹ The dihedral angles between the benzene and triazole moieties are 17 and 17.4°, while the dihedral angle between two terminal triazole rings is 92.6°, which indicates that the terminal triazole groups on each *cis*-TPPT ligand are basically perpendicular to each other and have much stronger spatial distortion than that of **1a**. Every Fe^{II} ion is connected by a TPPT ligand to form a 1D zigzag chain, and the neighboring 1D zigzag chains are linked to each other to ultimately afford a 1D layer (Figure S12). To the best of our knowledge, **1b** represents a 2D iron(II) triazole complex bridged by $\text{C}_2\text{O}_4^{2-}$ anions.

At room temperature, complex **1b** displays strong green fluorescence, as revealed in Figure S13. The highest emission band of **1b** is excited at $\lambda = 385$ nm and situates at $\lambda = 512$ nm. Compared with TPPT, the emission of complex **1b** is neither ligand-to-metal nor metal-to-ligand charge transfer. It can probably be assigned as an intraligand fluorescent emission because it has the same emission shape as the TPPT ligand. The rise of intraligand fluorescence in **1b** perhaps accounts for the coordination of TPPT to Fe^{II} , which enhances the conformation stiffness of TPPT and decreases the nonradiative decay of the intraligand ($\pi\text{--}\pi^*$) excited state.¹²

As displayed in Figure S14, complex **1b** shows wide cyan luminescence in the solution of DMF and the main emission band is located at $\lambda = 580$ nm (excited at $\lambda = 365$ nm). The fluorescent emissions may be assigned as an intraligand fluorescent emission because of the similar behavior in the TPPT ligand.^{8c} Coordination interaction gives rise to slight red

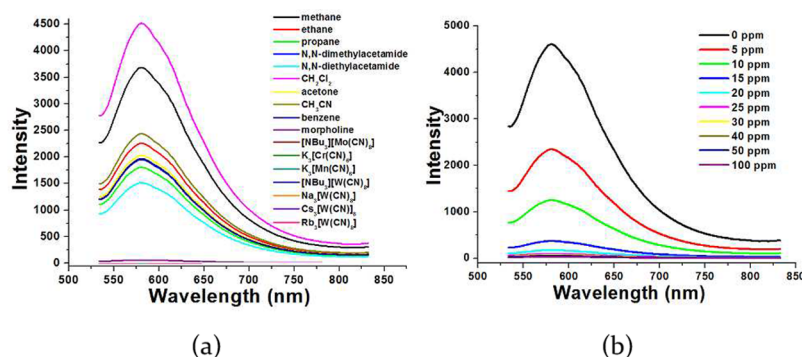


Figure 2. (a) Emission spectra of **1b** dispersed in DMF with the addition of different organic molecules and cyano groups (400 ppm). (b) Fluorescence titration of complex **1b** dispersed in DMF with the addition of different concentrations of $K_3[Cr(CN)_6]$.

shifts of the emissions. In comparison with the fluorescent emission of the TPPT solution, the emission of **1b** appears to narrow and red shifts, ascribed to an intermolecular mutual effect, most likely $\pi-\pi^*$ stacking interactions.

On the other hand, different anions were chosen to conduct the anion-sensing experiment on the basis of the cationic structure and porosity of **1b**. Various anions, such as Cl^- , NO_3^- , I^- , OAc^- , Br^- , ClO_4^- , SO_4^{2-} , CO_3^{2-} , BF_4^- , F^- , and CrO_4^{2-} , were immersed in the solution of **1b**. The luminescent properties demonstrate that various anions have a huge impact on the luminescent intensity of **1b**. It is noted that CrO_4^{2-} has the maximum quenching effect on the emission, as shown in Figure S15a. Although there have been a few published papers of anion exchange concerning MOFs, it is still rare to employ a cationic framework of Fe^{II} to study the fluorescence identification of pollutants.¹³ Hence, further research about the fluorescence probe of **1b** for the CrO_4^{2-} anion needs to be carried out. When placing **1b** (0.01 mmol) in K_2CrO_4 (0.005 mmol) along with gentle stirring, we implemented the exchange process at ambient temperature. Through liquid UV spectroscopy, the resultant solution can be detected from time to time. In a K_2CrO_4 solution, the absorption intensity of the main characteristic band ($\lambda = 375$ nm) decreased significantly with time, thus indicating that CrO_4^{2-} was gradually incorporated into the channel of **1b**. After **1b** was immersed in K_2CrO_4 for 12 h, the UV absorption intensity remained constant. The resultant concentration was reduced by 86.7%, as shown in Figure S15b. During the process of guest loading, the luminescent intensity of **1b** decreased slowly. At the same time, it was consistent with the inhibitory effect of the CrO_4^{2-} anion.

CrO_4^{2-} may also be absorbed onto the surface of **1b**. The mechanism of luminescence quenching may be as follows: Luminescent quenching of **1b** induced by CrO_4^{2-} anions may be ascribed to the interactions between CrO_4^{2-} anions and the network. This result came from competitive adsorption of the excitation wavelength energy between **1b** and CrO_4^{2-} .

Further, the addition of cyano moieties, for example, $K_3[Mn(CN)_6]$, $K_3[Cr(CN)_6]$, $Na_3[W(CN)_8]$, $Na_3[Mo(CN)_8]$, $Cs_3[W(CN)_8]$, $[NBu_3][W(CN)_8]$, $Rb_3[W(CN)_8]$, and $[NBu_3][Mo(CN)_8]$, to a concentration of 400 ppm nearly reduced the intensity of **1b** to zero, as illustrated in Figure 2a. However, the greatest change of the intensity was just 67.4% upon the addition of an equal amount of other organic molecules, incorporating amides, chloroalkanes, alcohols, nitriles, ketones, and even some aromatic and heterocyclic compounds. The luminescent properties demonstrated that **1b** can be viewed as a selective probe for cyano moieties, especially for $K_3[Cr(CN)_6]$. In order to further

study the sensor characteristics of **1b**, the dynamic response was guided by the addition of $K_3[Cr(CN)_6]$ little by little in the dispersed **1b** in DMF. After the addition of $K_3[Cr(CN)_6]$ with a concentration of 5 ppm, the emission intensity of **1b** decreased and was almost destroyed to about zero at 100 ppm. The quenching efficiency is as high as 99.33%, as shown in Figure 2b.

In summary, a SC-SC transformation induced by anion and solvent exchange has been demonstrated to generate the 2D iron(II) triazole layer **1b** containing $C_2O_4^{2-}$ bridges. More interestingly, **1b** can be considered to be a promising luminescent probe for CrO_4^{2-} and cyano molecules based on triazole derivatives.

■ ASSOCIATED CONTENT

📄 Supporting Information

The Supporting Information is available free of charge on the ACS Publications website at DOI: 10.1021/acs.inorgchem.7b03047.

Listings of the synthesis, general methods, tables of crystal data, supplementary figures, thermogravimetric analysis plots, luminescent properties, 1H NMR, and PXRD results (PDF)

Accession Codes

CCDC 1525240–1525242 contain the supplementary crystallographic data for this paper. These data can be obtained free of charge via www.ccdc.cam.ac.uk/data_request/cif, or by emailing data_request@ccdc.cam.ac.uk, or by contacting The Cambridge Crystallographic Data Centre, 12 Union Road, Cambridge CB2 1EZ, UK; fax: +44 1223 336033.

■ AUTHOR INFORMATION

Corresponding Author

*E-mail: wangying790601@163.com.

ORCID

Ying Wang: 0000-0002-8126-3325

Notes

The authors declare no competing financial interest.

■ ACKNOWLEDGMENTS

This work was supported financially by the NSFC (Grant 21471113), Training Program of Outstanding Youth Innovation Team of Tianjin Normal University, National Top-Level Talent Training Program of Tianjin Normal University, 111 Project (B12015), and Opening Fund of Key Laboratory of Advanced Energy Materials Chemistry (Ministry of Education), Nankai University.

REFERENCES

- (1) (a) Zhou, H.-C.; Long, J. R.; Yaghi, O. M. Introduction to Metal-Organic Frameworks. *Chem. Rev.* **2012**, *112*, 673. (b) Li, W.-Y.; Xu, L.-N.; Chen, J. Co₃O₄ Nanomaterials in Lithium-Ion Batteries and Gas Sensors. *Adv. Funct. Mater.* **2005**, *15*, 851–857. (c) Li, X.; Zhang, G.; Cheng, F.; Guo, B.; Chen, J. Synthesis, Characterization, and Gas-Sensor Application of WO₃ Nanocuboids. *J. Electrochem. Soc.* **2006**, *153*, H133–H137. (d) Cohen, S. M. Postsynthetic Methods for the Functionalization of Metal-Organic Frameworks. *Chem. Rev.* **2012**, *112*, 970–1000. (e) Sun, Q.; Aguila, B.; Perman, J.; Earl, L. D.; Abney, C. W.; Cheng, Y.; Wei, H.; Nguyen, N.; Wojtas, L.; Ma, S. Postsynthetically Modified Covalent Organic Frameworks for Efficient and Effective Mercury Removal. *J. Am. Chem. Soc.* **2017**, *139*, 2786–2793. (f) Li, B.; Sun, Q.; Zhang, Y.; Abney, C. W.; Aguila, B.; Lin, W.; Ma, S. *ACS Appl. Mater. Interfaces* **2017**, *9*, 12511–12517. (g) Zhou, H. C.; Kitagawa, S. Metal-Organic Frameworks (MOFs). *Chem. Soc. Rev.* **2014**, *43*, 5415–5418. (h) Chen, B.; Xiang, S.; Qian, G. Metal-Organic Frameworks with Functional Pores for Recognition of Small Molecules. *Acc. Chem. Res.* **2010**, *43*, 1115–1124. (i) Getman, R. B.; Bae, Y. S.; Wilmer, C. E.; Snurr, R. Q. Review and Analysis of Molecular Simulations of Methane, Hydrogen, and Acetylene Storage in Metal-Organic Frameworks. *Chem. Rev.* **2012**, *112*, 703–723. (j) Horcajada, P.; Gref, R.; Baati, T.; Allan, P. K.; Maurin, G.; Couvreur, P.; Ferey, G.; Morris, R. E.; Serre, C. Metal-Organic Frameworks in Biomedicine. *Chem. Rev.* **2012**, *112*, 1232–1268. (k) Kreno, L. E.; Leong, K.; Farha, O. K.; Allendorf, M.; Van Duyne, R. P.; Hupp, J. T. Metal-Organic Framework Materials as Chemical Sensors. *Chem. Rev.* **2012**, *112*, 1105–1125. (l) Lee, J.; Farha, O. K.; Roberts, J.; Scheidt, K. A.; Nguyen, S. T.; Hupp, J. T. Metal-organic framework materials as catalysts. *Chem. Soc. Rev.* **2009**, *38*, 1450–1459. (m) Suh, M. P.; Park, H. J.; Prasad, T. K.; Lim, D. W. Hydrogen Storage in Metal-Organic Frameworks. *Chem. Rev.* **2012**, *112*, 782–835. (n) Lin, R.-B.; Liu, S.-Y.; Ye, J.-W.; Li, X.-Y.; Zhang, J.-P. Photoluminescent Metal-Organic Frameworks for Gas Sensing. *Adv. Sci.* **2016**, *3*, 1500434.
- (2) (a) Wang, H.; Meng, W.; Wu, J.; Ding, J.; Hou, H.; Fan, Y. Crystalline central-metal transformation in metal-organic frameworks. *Coord. Chem. Rev.* **2016**, *307*, 130–146. (b) Meng, W.; Li, H.; Xu, Z.; Du, S.; Li, Y.; Zhu, Y.; Han, Y.; Hou, H.; Fan, Y.; Tang, M. New Mechanistic Insight into Stepwise Metal-Center Exchange in a Metal-Organic Framework Based on Asymmetric Zn₄ Clusters. *Chem. - Eur. J.* **2014**, *20*, 2945–2952. (c) Han, Y.; Chilton, N. F.; Li, M.; Huang, C.; Xu, H.; Hou, H.; Moubaraki, B.; Langley, S. K.; Batten, S. R.; Fan, Y.; Murray, K. S. Post-Synthetic Monovalent Central-Metal Exchange, Specific I₂ Sensing, and Polymerization of a Catalytic [3 × 3] Grid of [Cu^{II}₃Cu^I₄L₆](I)₂·13H₂O. *Chem. - Eur. J.* **2013**, *19*, 6321–6328. (d) Kitagawa, D.; Kawasaki, K.; Tanaka, R.; Kobatake, S. Mechanical Behavior of Molecular Crystals Induced by Combination of Photochromic Reaction and Reversible Single-Crystal-to-Single-Crystal Phase Transition. *Chem. Mater.* **2017**, *29*, 7524–7532. (e) Sharma, V.; De, D.; Pal, S.; Saha, P.; Bharadwaj, P. K. A 2D Coordination Network That Detects Nitro Explosives in Water, Catalyzes Baylis-Hillman Reactions, and Undergoes Unusual 2D→3D Single-Crystal to Single-Crystal Transformation. *Inorg. Chem.* **2017**, *56*, 8847–8855. (f) Korzeniak, T.; Jankowski, R.; Koziel, M.; Pinkowicz, D.; Sieklucka, B. Reversible Single-Crystal-to-Single-Crystal Transformation in Photomagnetic Cyanido-Bridged Cd₄M₂ Octahedral Molecules. *Inorg. Chem.* **2017**, *56*, 12914–12919.
- (3) (a) Park, I.-H.; Medishetty, R.; Lee, H.-H.; Mulijanto, C. E.; Quah, H. S.; Lee, S. S.; Vittal, J. J. Formation of a Syndiotactic Organic Polymer Inside a MOF by a [2 + 2] Photo-Polymerization Reaction. *Angew. Chem., Int. Ed.* **2015**, *54*, 7313–7317. (b) Chatterjee, P. B.; Audhya, A.; Bhattacharya, S.; Abtab, S. M. T.; Bhattacharya, K.; Chaudhury, M. Single Crystal-to-Single Crystal Irreversible Transformation from a Discrete Vanadium(V)-Alcoholate to an Aldehydic-Vanadium(IV) Oligomer. *J. Am. Chem. Soc.* **2010**, *132*, 15842–15845. (c) Wei, Y.-S.; Zhang, M.; Liao, P.-Q.; Lin, R.-B.; Li, T.-Y.; Shao, G.; Zhang, J.-P.; Chen, X.-M. Coordination templated [2 + 2+2] cyclotrimerization in a porous coordination framework. *Nat. Commun.* **2015**, *6*, 8348. (f) Tian, J.; Saraf, L. V.; Schwenzler, B.; Taylor, S. M.; Brechin, E. K.; Liu, J.; Dalgarno, S. J.; Thallapally, P. K. Selective Metal Cation Capture by Soft Anionic Metal-Organic Frameworks via Drastic Single-Crystal-to-Single-Crystal Transformations. *J. Am. Chem. Soc.* **2012**, *134*, 9581–9584.
- (4) (a) Yuan, S.; Zou, L.; Qin, J.-S.; Li, J.; Huang, L.; Feng, L.; Wang, X.; Bosch, M.; Alsalmeh, A.; Cagin, T.; Zhou, H.-C. Construction of hierarchically porous metal-organic frameworks through linker labilization. *Nat. Commun.* **2017**, *8*, 15356. (b) Yuan, S.; Chen, Y.-P.; Qin, J.-S.; Lu, W.; Zou, L.; Zhang, Q.; Wang, X.; Sun, X.; Zhou, H.-C. Linker Installation: Engineering Pore Environment with Precisely Placed Functionalities in Zirconium MOFs. *J. Am. Chem. Soc.* **2016**, *138*, 8912–8919. (c) Yuan, S.; Zou, L.; Li, H.; Chen, Y.-P.; Qin, J.; Zhang, Q.; Lu, W.; Hall, M. B.; Zhou, H.-C. Flexible Zirconium Metal-Organic Frameworks as Bioinspired Switchable Catalysts. *Angew. Chem., Int. Ed.* **2016**, *55*, 10776–10780. (d) Yuan, S.; Qin, J.-S.; Zou, L.; Chen, Y.-P.; Wang, X.; Zhang, Q.; Zhou, H.-C. Thermodynamically Guided Synthesis of Mixed-Linker Zr-MOFs with Enhanced Tunability. *J. Am. Chem. Soc.* **2016**, *138*, 6636–6642.
- (5) Zou, Y.; Wang, X.; Khan, A.; Wang, P.; Liu, Y.; Alsaedi, A.; Hayat, T.; Wang, X. Environmental remediation and application of nanoscale zero-valent iron and its composites for the removal of heavy metal ions: a review. *Environ. Sci. Technol.* **2016**, *50*, 7290.
- (6) Webster, O. W. Cyanocarbons: A classic example of discovery-driven research. *J. Polym. Sci., Part A: Polym. Chem.* **2002**, *40*, 210–221.
- (7) Danielsson, J.; Meuwly, M. Energetics and Dynamics in MbCN: CN⁻-Vibrational Relaxation from Molecular Dynamics Simulations. *J. Phys. Chem. B* **2007**, *111*, 218–226.
- (8) (a) Wang, Y.; Jia, W.; Chen, R.; Zhao, X.-J.; Wang, Z.-L. Guest-induced SC–SC transformation within the first K/Cd heterodimetallic triazole complex: a luminescent sensor for high-explosives and cyano molecules. *Chem. Commun.* **2017**, *53*, 636–639. (b) Wang, Y.; Yi, J.-M.; Zhang, M.-Y.; Xu, P.; Zhao, X.-J. I₂-induced SC–SC transformation within two-dimensional Zn(II)-triazole framework: an ideal detector of cyano-containing molecules. *Chem. Commun.* **2016**, *52*, 3099–3102. (c) Wang, Y.; Xu, P.; Xie, Q.; Ma, Q.-Q.; Meng, Y.-H.; Wang, Z.-W.; Zhang, S.; Zhao, X.-J.; Chen, J.; Wang, Z.-L. Cadmium(II)-Triazole Framework as a Luminescent Probe for Ca²⁺ and Cyano Complexes. *Chem. - Eur. J.* **2016**, *22*, 10459–10474. (d) Wang, Y.; Meng, S.-S.; Lin, P.-X.; Xiao, Y.-W.; Ma, Q.-Q.; Xie, Q.; Chen, Y.-Y.; Zhao, X.-J.; Chen, J. Solvent-Induced Single Crystal–Single Crystal Transformation of an Interpenetrated Three-Dimensional Copper Triazole Catalytic Framework. *Inorg. Chem.* **2016**, *55*, 4069–4071. (e) Wang, Y.; Cheng, L.; Liu, Z.-Y.; Wang, X.-G.; Ding, B.; Yin, L.; Zhou, B.-B.; Li, M.-S.; Wang, J.-X.; Zhao, X.-J. An Ideal Detector Composed of Two-Dimensional Cd(II)-Triazole Frameworks for Nitro-Compound Explosives and Potassium Dichromate. *Chem. - Eur. J.* **2015**, *21*, 14171–14178. (f) Wang, Y.; Yuan, B.; Xu, Y.-Y.; Wang, X.-G.; Ding, B.; Zhao, X.-J. Turn-On Fluorescence and Unprecedented Encapsulation of Large Aromatic Molecules within a Manganese(II)-Triazole Metal-Organic Confined Space. *Chem. - Eur. J.* **2015**, *21*, 2107–2116. (g) Wang, Y.; Wang, X.-G.; Yuan, B.; Shao, C.-Y.; Chen, Y.-Y.; Zhou, B.-B.; Li, M.-S.; An, X.-M.; Cheng, P.; Zhao, X.-J. Cation-Exchange Porosity Tuning in a Dynamic 4d–4f–3d Framework for Ni^{II} Ion-Selective Luminescent Probe. *Inorg. Chem.* **2015**, *54*, 4456–4465. (h) Liu, J.-Y.; Wang, Q.; Zhang, L.-J.; Yuan, B.; Xu, Y.-Y.; Zhang, X.; Zhao, C.-Y.; Wang, D.; Yuan, Y.; Wang, Y.; Ding, B.; Zhao, X.-J.; Yue, M. M. Anion-Exchange and Anthracene-Encapsulation within Copper(II) and Manganese(II)-Triazole Metal-Organic Confined Space in a Single Crystal-to-Single Crystal Transformation Fashion. *Inorg. Chem.* **2014**, *53*, 5972–5985.
- (9) (a) Wang, Y.-X.; Qiu, D.; Xi, S.-F.; Ding, Z.-D.; Li, Z.; Li, Y.; Ren, X.; Gu, Z.-G. Iron(II)-triazole core–shell nanocomposites: toward multistep spin crossover materials. *Chem. Commun.* **2016**, *52*, 8034–8037. (b) Yan, Z.; Liu, W.; Peng, Y.-Y.; Chen, Y.-C.; Li, Q.-W.; Ni, Z.-P.; Tong, M.-L. Spin-Crossover Phenomenon in a Pentanuclear Iron(II) Cluster Helicate. *Inorg. Chem.* **2016**, *55*, 4891–4896.
- (10) Desiraju, G. R.; Steiner, T. *The Weak Hydrogen Bond in Structural Chemistry and Biology*; Oxford University Press: Oxford, U.K., 1999.
- (11) (a) Spek, A. L. *PLATON: A Multipurpose Crystallographic Tool*; University of Utrecht: Utrecht, The Netherlands, 2001. (b) Blatov, V. A.; Shevchenko, A. P.; Proserpio, D. M. Applied Topological Analysis of

Crystal Structures with the Program Package Topos Pro. *Cryst. Growth Des.* **2014**, *14*, 3576–3586.

(12) Haasnoot, J. G. Mononuclear, oligonuclear and polynuclear metal coordination compounds with 1,2,4-triazole derivatives as ligands. *Coord. Chem. Rev.* **2000**, *200–202*, 131–185.

(13) (a) Yi, F.-Y.; Li, J.-P.; Wu, D.; Sun, Z.-M. A Series of Multifunctional Metal–Organic Frameworks Showing Excellent Luminescent Sensing, Sensitization, and Adsorbent Abilities. *Chem. - Eur. J.* **2015**, *21*, 11475–11482. (b) Liu, W.; Wang, Y.; Bai, Z.; Li, Y.; Wang, Y.; Chen, L.; Xu, L.; Diwu, J.; Chai, Z.; Wang, S. Hydrolytically Stable Luminescent Cationic Metal Organic Framework for Highly Sensitive and Selective Sensing of Chromate Anions in Natural Water Systems. *ACS Appl. Mater. Interfaces* **2017**, *9*, 16448–16457.